frontiers in Chemistry

ORIGINAL RESEARCH
published: 05 May 2020
doi: 10.3389/fchem.2020.00365

Photocatalytic Degradation of Aqueous Rhodamine 6G Using Supported TiO_2 Catalysts. A Model for the Removal of Organic Contaminants From Aqueous Samples

Eduardo Pino [1], Cristian Calderón [1]*, Francisco Herrera [1], Gerardo Cifuentes [2] and Gisselle Arteaga [3]*

[1] Facultad de Química y Biología, Universidad de Santiago de Chile, Santiago, Chile, [2] Departamento de Ingeniería Metalúrgica, Universidad de Santiago de Chile, Santiago, Chile, [3] Departamento de Ingeniería Química, Universidad de Santiago de Chile, Santiago, Chile

OPEN ACCESS

Edited by:
Kamila Kočí, VŠB-Technical University of Ostrava, Czechia

Reviewed by:
Guohong Wang, Hubei Normal University, China
Sebastián Murcia-López, Institut de Recerca de l'Energia de Catalunya, Spain
Yi-en Du, Jinzhong University, China

***Correspondence:**
Eduardo Pino
eduardo.pino@usach.cl
Cristian Calderón
cristian.calderon@usach.cl

Specialty section:
This article was submitted to Catalysis and Photocatalysis, a section of the journal Frontiers in Chemistry

Received: *13 November 2019*
Accepted: *08 April 2020*
Published: *05 May 2020*

Citation:
Pino E, Calderón C, Herrera F, Cifuentes G and Arteaga G (2020) Photocatalytic Degradation of Aqueous Rhodamine 6G Using Supported TiO_2 Catalysts. A Model for the Removal of Organic Contaminants From Aqueous Samples. Front. Chem. 8:365. doi: 10.3389/fchem.2020.00365

As a model for the removal of complex organic contaminants from industrial water effluents, the heterogeneous photocatalytic degradation of Rhodamin 6G was studied using TiO_2-derived catalysts, incorporated in water as suspension as well as supported in raschig rings. UV and Visible light were tested for the photo-degradation process. TiO_2 catalysts were synthesized following acid synthesis methodology and compared against commercial TiO_2 catalyst samples (Degussa P25 and Anatase). The bandgap (E_g) of the TiO_2 catalysts was determined, were values of 2.97 and 2.98 eV were obtained for the material obtained using acid and basic conditions, respectively, and 3.02 eV for Degussa P25 and 3.18 eV for anatase commercial TiO_2 samples. Raschig rings-supported TiO_2 catalysts display a good photocatalytic performance when compared to equivalent amounts of TiO_2 in aqueous suspension, even though a large surface area of TiO_2 material is lost upon support. This is particularly evident by taking into account that the characteristics (XRD, RD, Eg) and observed photodegradative performance of the synthesized catalysts are in good agreement with the commercial TiO_2 samples, and that the RH6G photodegradation differences observed with the light sources considered are minimal in the presence of TiO_2 catalysts. The presence of additives induce changes in the kinetics and efficiency of the TiO_2-catalyzed photodegradation of Rh6G, particularly when white light is used in the process, pointing toward a complex phenomenon, however the stability of the supported photocatalytic systems is acceptable in the presence of the studied additives. In line with this, the magnitude of the chemical oxygen demand, indicates that, besides the different complex photophysical processes taking place, the endproducts of the considered photocatalytic systems appears to be similar.

Keywords: photocatalytic degradation, organic dyes, water treatment, contaminant, semiconductor sensitizer

INTRODUCTION

The removal of hazardous organic contaminants derived from human productive activities, present in the environment and particularly in water sources has become an important research topic aimed toward the development of sustainable water treatment strategies and processes.

The leather, paper, plastic and textile industries use dyes to color their products while using large volumes of water (Robinson et al., 2001; Yaseen and Scholz, 2019), with more than 10,000 types of commercial dyes and 70,000 tons of waste are produced annually. This discharge of wastewater to natural streams leads to major problems, such as an increase in toxicity and oxygen demand of the effluents, as well as a reduction of the amount of light that can pass through the water, producing a negative effect on the phenomena of photosynthesis of aquatic life. The color of wastewater is the first public perception of contamination, the presence of small amounts of dyes (1 ppm) is highly visible and undesirable, due to their high molar absorptivity coefficients.

For the vast array of wastewater treatment technologies currently in use, namely adsorption on activated carbon (Foo and Hameed, 2009), ultrafiltration, coagulation by chemical agents and resins of synthetic adsorbents, biological treatment, electrocatalytic decomposition (Fujishima and Honda, 1972; Daghrir et al., 2012), etc., factors such as the sheer complexity of the organic contaminants found in waste water effluents call for a simpler yet transversal solution, able to yield a proper removal of the contaminants by an aggressive oxidative decomposition. From this, advanced oxidation processes (AOPs) for chemical degradation have become simple and effective methods for the elimination of organic contaminants (Giménez et al., 2015).

Several research groups have sought to optimize the process for the degradation of organic pollutants in water (Rizzo et al., 2009; Chong et al., 2010), so that it meets the requirements of efficiency, easy to handle, and improved time of degradation, by allowing the pollutants complete mineralization, that is, the formation of carbon dioxide (CO_2), water (H_2O) and other inorganic compounds such as HCl, HNO_3, etc. and/or the generation of less toxic organic byproducts that are environmentally safe (Amenn et al., 2013). Based on this premise, photocatalytic degradation has become a widespread subject of study, focused on making use of the particular interactions that takes place between light and semiconductive materials (SCM), in a process termed as heterogeneous photocatalysis (Ahmed et al., 2011; Teoh et al., 2012), that allows the degradation of organic molecules via advanced oxidative pathways, due to the abundant generation of radicals on the surface of the SCM by electronic excitation elicited by the incident light.

Heterogeneous photocatalysis, has become an efficient alternative to achieve the degradation of many pollutants. This technique uses radiant energy, visible and / or ultraviolet light coming from artificial light sources or directly from the sun, which, upon interacting with a catalyst (semiconductor) (Smith and Nie, 2009), generates a charge separation by means of charge transfer processes, leading to the formation of reactive oxygen species (hydroxyl radicals, superoxide anion, hydrogen peroxide, etc.), necessary for the oxidation and subsequent mineralization of the organic contaminants (Módenes et al., 2012).

One of the most efficient SCM, in terms of both cost and photocatalytic properties, is Titanium dioxide (TiO_2) with a large number of works published elsewhere (Ajmal et al., 2014; Gaya, 2014), devoted to in-deep descriptions of the interesting photophysical properties of this material. Briefly, the ability of SCM such as TiO_2 to be activated by photon absorption is associated to the energy difference, or bandgap (Eg) that separates their valence band (VB) electrons from their counterparts in the conduction band (CB), where Eg is usually lower than 5 eV in common SCM (Smith and Nie, 2009). Upon light excitation, electrons move from VB to CB, leaving a hole (h^+) into the VB. Further, the transferred electrons can participate in the generation of reactive oxygen species (ROS), leading to occurrence of photocatalytic degradation. A general description of the photocatalytic degradation of dyes in the presence of TiO_2 is shown in Equations (1–6).

$$TiO_2 + h\nu\,(UV) \rightarrow TiO_2\left(e^-_{CB} + h^+_{VB}\right) \quad (1)$$

$$TiO_2\left(h^+_{VB}\right) + H_2O \rightarrow TiO_2 + H^+ + OH^\bullet \quad (2)$$

$$TiO_2\left(h^+_{VB}\right) + HO^- \rightarrow TiO_2 + OH^\bullet \quad (3)$$

$$TiO_2\left(e^-_{CB}\right) + O_2 \rightarrow TiO_2 + O_2^{\bullet-} \quad (4)$$

$$O_2^{\bullet-} + H^+ \rightarrow HO_2^\bullet \rightarrow H_2O_2 \rightarrow OH^\bullet \quad (5)$$

$$Dye + ROS \rightarrow Products \quad (6)$$

TiO_2 has three crystalline phases, anatase (tetragonal), rutile (octahedral) and brookite (orthorhombic) (Landmann et al., 2012), with anatase being the most active photocatalytically due to the combined effect of a lower recombination rate and a higher capacity of adsorption on the surface (Carreon et al., 2011). The TiO_2 in mixed phase have a greater photocatalytic activity compared to a pure crystalline phase (Hurum et al., 2003). TiO_2 use is limited by fact that the absorption of light corresponding to the Eg for the cristalline forms of TiO_2 falls in the ultraviolet range, which is one of the minority components of the solar spectrum. This disadvantage of the semiconductor is due to its high value of Eg, being 3.2 eV for anatase and 3.02 eV for rutile. To extend the range of absorption of the catalysts to the visible spectrum and decrease the recombination of the pair (h^+_{VB} / e^-_{CB}) one of the strategies used has been the use of photosensitizing dyes (Stracke and Heupel, 1999). Upon irradiation, the transfer of electrons from the excited state of the dye to the conduction band of the semiconductor can be produced, in a process defined as "sensitization" (equations 7-19) of the TiO_2 (Wu et al., 1998). This process only will be possible if the energy level of the excited state of the dye (Dye*) is higher than the energy level of the conduction band. The injected electrons can be transferred to the oxygen adsorbed on the TiO_2 surface to form superoxide anion radicals, which lead to the formation of ROS (Dyi-Hwa et al., 2012), these species being responsible for the oxidation of organic matter (Song et al., 2016). The sensitizing dye is also degraded in the process (equations 5 and 6), making this synergy between the sensitizing dye and TiO_2, ideal for the decomposition of organic contaminants able to sensitize TiO_2 using white light, minimizing

the use of high energy radiation (ca. UV light) by ignoring the Eg value of the photocatalyst.

$$Dye + hv \rightarrow Dye^{*} \quad (7)$$

$$Dye^{*} \rightarrow bleaching\ or\ photophysical\ process \quad (8)$$

$$TiO_2 + Dye^{*}\left(e^{-}\right) \rightarrow TiO_2\left(e^{-}_{cb}\right) + Dye^{\bullet +} \rightarrow Products \quad (9)$$

Besides of taking advantage of the dye-sensitizing of TiO_2, and in order to further extend the applications and usability of TiO_2 catalysts, the support of the photocatalytic material have become an interesting venture for catalysis research. Current developments for the use TiO_2 are focused on the support of the photocatalyst on a wide variety of materials (Ansón-Casaos et al., 2013; Ranjith et al., 2019) which may set the basis for the implementation of applied waste-water treatment solutions. Polymeric supports have been considered to enhance and control the photocatalytic properties of TiO_2. Recently, poly (ethyleneterephtalate)-supported TiO_2 composite films (Malesic-Eleftheriadou et al., 2019) have proven useful for the photocatalytic degradation of complex antibiotic mixtures irradiated with simulated solar light, leading to high photocatalytic efficiencies and good reusability even when low content (10%) of supported TiO_2 is used. Hyerarchical wrinkled mesoporous silica used as support for TiO_2 catalysts (Wan et al., 2018), have shown high TiO_2 support yield and enhanced photodegradation activity toward organic dyes, particularly the TiO_2 catalyzed photodegradation of Rhodamin B under UV light exposition, where the performance of the supported catalyst can be modulated by controlling the calcination temperature during the TiO_2 support step.

Studies evaluating the performance of metal oxide nanoparticles/TiO2 heterojunctions have reported an enhanced degradation of Rhodamine B. For example, ZnO/TiO_2 heterojunction photocatalysts (Wang et al., 2018), in a degradation process mediated by the formation of a direct Z-scheme heterojunction structure formed between ZnO and TiO_2, with hydroxyl and superoxide anion radical playin relevant roles in the phtocatalytic process. Similarly, enhanced photocatalytic performance under visible light irradiation have been observed for p-n heterojunctions formed in TiO_2 nanofibers decorated with Ag_2O nanoparticles (Liu et al., 2019), effect mainly attributed to the fast separation of the photogenerated electron-hole pairs and high light absorption efficiency of the fibers. On the other hand, nanophotocatalysts based on $TiO_2/SrTiO_3$ heterojunctions supported on activated carbon (Ali et al., 2019) have displayed exceptional activities, compared to commercial TiO_2 samples, on the photodegradation of pollutants such as 2,4-dichlorophenol and bisphenol A, where the presence of the activated carbon allows the enhancement of the photocatalystic activity by increasing the adsorption of O_2, as well as by accepting the electrons from the semiconductors heterojunction.

Degussa-P25 TiO_2 catalyst supported on mullite ceramic foam was tested in a photocatalytic ozonization process for the degradation of N-N-diethyl-m-toluamide (Rodríguez et al., 2019). The performance of the mullite supported catalysts was close to that observed when raschig rings where used as support, where the combination of the ozone and TiO_2 photocatalyzed degradation had a negative impact on the degradation rate, but higher efficiency on the mineralization process of the substrate.). TiO_2 supported in activated carbon has also been used for the photocatalytic decomposition of the micotoxin aflatoxin B1 (Sun et al., 2019), a carcinogen agent that can be found in vegetal and animal feedstock, with good performance of the photocatalyst when UV-Vis light is used for irradiation, with enhanced photodegradation of the supported material when compared with the bare photocatalysts. Similarly, hybrid TiO_2 catalysts supported on reduced graphene oxide (Ranjith et al., 2019) displayed good performance in the oxidative degradation of organic dyes (methylene blue and crystal violet) by irradiation with visible light, with the dye degradation taking place through electron-hole separation.

Beyond the development of TiO_2 supported in microgranular porous materials, larger structures of supporting material have been less explored. For example, periodic and flow reactors using TiO_2 catalysts in suspension as well as supported on glass fabric have been used for the UV-Vis photocatalyzed degradation of sertraline, an antidepressant drug, from aqueous samples (Rejek and Grzechulska-Damszel, 2018). The photodegradation yield where highly dependent on the configuration of photoreactor, where the highest degradation percentages where achieved using the periodic reactor containing the TiO_2-coated glass fabric. TiO_2 coated natural and synthetic non-woven fibers have also been tested on the photocatalyzed degradation of the textile dye reactive yellow 145 (Alahiane et al., 2014) where good degradation performance under irradiation with UV light, was achieved under several conditions, such as the presence of additives, namely ethanol, hydrogen peroxide, inorganic anions, as well as optimal degradation in acidic media ($pH = 3$).

The present work will focus on the study of TiO_2 catalysts supported on borosilicate glass rings (raschig rings), which will allow the development and optimization of a photocatalytic degradation process based on the use of both UV and white light, taking advantage of the ability of the different crystal structures of TiO_2, leading to a controllable photodegradation process of complex organic molecules by control of the free radical generation process on the supported TiO_2 catalysts, either by the energy of the incident light or the combination of different TiO_2 crystal structures, allocated on the vitreous support. The physically and chemically stable supported photocatalytic structures will yield reusable materials for the implementation of water decontamination strategies either for batch or continuous regime water treatment, providing stability to the TiO_2 particles, enhancement of the catalytic surface to the incident light as well as adsorption of the substrates for the degradation, combined with good mass transport through the material, by taking advantage of the intrinsic properties of the design of the raschig rings as packing material, for example, in engineering application of fractionation columns (Raja et al., 2005).

Due to the fact that colored dyes, commonly found as waste water organic contaminants usually share similarities in their structures, a model compound is required in order to test the proposed TiO_2 catalysts in a streamlined and proper fashion (Lasio et al., 2013; Bokhale et al., 2014), allowing

further analysis and interpretation of the obtained results. In this context, xanthenic dyes stands out as a suitable candidates. Rhodamine 6G (Rh6G) also known as Rhodamine 590, belongs to the xanthenes family, which are largely used to synthesize drugs and to prepare dyes of the fluorescein and eosin class. Rhodamine 6G is a cationic polar dye with a rigid heterocyclic structure, which exhibits a strong absorption in the visible and an intense fluorescence (Magde et al., 1999; Bujdak and Iyi, 2012; Zehentbauer et al., 2014). Rh6G is widely used in acrylic, nylon, silk, wool and dyeing, it is the dye most used for dye laser applications and as a fluorescent tracer to visualize flow patterns as for example in the field of hydraulics (Tarud et al., 2010). Rh6G is commonly used as a sensitizer (Wu et al., 1998). In recent years, a growing number of studies have attempted to incorporate Rh6G into inorganic and organic matrices (Vanamudan and Pamidimukkala, 2015) for application in fields such as solid-state laser action, optoelectronics and optical filters, among others (Barranco and Groening, 2006).

Our analysis comprises the use of TiO_2 catalysts synthesized by a sol-gel methodology, as well as commercial samples of TiO_2 (Anatase and Degussa P25) supported in raschig rings and the photocatalytic activity of the supported catalysts evaluated by monitoring the degradation of Rh6G under irradiation with UV (365 nm) and white light (400–700 nm) light sources. Further, the influence of additives that can be usually found accompanying organic dyes in waste water, such as sulfates and chlorides (Guillard et al., 2005), as well as photocatalysis promoters such as hydrogen peroxide (Li et al., 2001), will be evaluated in our photocatalytic systems.

EXPERIMENTAL

Materials

Nitric Acid, titanium dioxide (Anatase), titanium dioxide (Degussa P25), titanium isopropoxide, polyethylene graft maleic anhydride and Rhodamin 6G were purchased from Sigma-Aldrich. Sodium chloride, n-hexane, sodium hydroxide, hydrogen peroxide and sodium sulfate were purchased from Merck. All reagents were used as received.

Methods

Synthesis of TiO_2

The synthesis of TiO_2 was performed by the Sol-gel method (Ochoa et al., 2009). A mixture of 100 mL of ultrapure water and 27 mL of isopropanol was used to dissolve 16.6 ml of titanium isopropoxide (Mahshid et al., 2007), under constant stirring for 20 min. Later, depending of the acidity required, 3.1 mL HNO_3 0.032 M (acid synthesis) were added and the suspension kept under constant stirring at 80°C for 20 hrs. Finally, the resulting gel was treated in a muffle furnace for 4 h at 560°C and then left to cool at room temperature to recover the solid TiO_2.

TiO_2 Support on Raschig Rings

In a crystallizer containing 0.25 g of polyethylene graft maleic anhydride (PEGMA), completely dissolved in 25 mL of hexane, 50 Raschig rings were incorporated and the temperature raised up to 70°C to achieve total evaporation of the solvent. The dried rings were added to an aqueous TiO_2 suspension (10 g/L for the synthesized TiO_2 catalysts or 1 g/L for the commercial TiO_2 samples) and left to rest for 30 min. Later, the solvent was evaporated by heating the suspension at 150°C followed by elimination of residual organic matter by heating at 500°C for 2 h in a muffle furnace (Raja et al., 2005). The TiO_2 support efficiency was calculated by determining the amount of TiO_2 supported on the rings (the total amount of rings used on the support step) by weight differences, and the resulting mass of TiO_2 supported was expressed as a percentage in relation to the total mass of TiO_2 used in the support step.

Characterization of the TiO_2 Catalysts

X-ray diffraction analysis of the synthesized TiO_2 catalysts were performed in order to discriminate the crystal structures present in the resulting material, and the results were compared with commercial TiO2 samples. XRD data was obtained using a Shimadzu XRD-6000 (Cu, Kα, Ni Filter, 40 kV, 30 mA) difractometer, with a 2 min^{-1} scan speed. Scanning electronic microcopy (SEM) analysis of the samples was performed in a JEOL JSM-7800F scanning electron microscope equipped wtih a X-ACT Cambridge instruments detector for energy dispersive X-ray (EDX) analysis.

BET adsorption isotherms and specific surface area of the studied TiO_2 catalysts were determined by using a Micromeritics ASAP 2020 systing, with N_2 gas as adsorbate at 77K.

The bandgap energy (Eg) of the synthesized TiO_2 catalysts was determined by diffuse reflectance experiments (López and Gómez, 2012), using the Kubelka-Munk function (FKM) for the analysis of the diffuse reflectance (R) of TiO_2, according to Equations (1, 2).

$$R = \frac{R_{sample}}{R_{reference}} \tag{1}$$

$$FKM = F(R) = \frac{(1-R)^2}{2R} \tag{2}$$

The Tauc mathematical model was used for the accurate determination of the Eg values. Briefly, this model proposes that, for materials with a direct band gap [REF], the magnitude of Eg can be estimated by Equation 3.

$$\alpha h\upsilon = A(h\upsilon - E_g)^n \tag{3}$$

Where ν is the frequency of the incident light, A correspond to a proportionality constant and α is a linear absorption coefficient. For TiO_2 and other materials with direct band gap, n is equal to 2 (Smith and Nie, 2009; López and Gómez, 2012). Under specific conditions, the absorption coefficient α is proportional to the FKM, according to Equation 4.

$$F(R)\, h\upsilon = A(h\upsilon - E_g)^n \tag{4}$$

From plots of $F(R)\, h\upsilon^{1/2}$ vs. $h\upsilon$, the linear extrapolation at $F(R)\, h\upsilon^{1/2} = 0$ allows the determination of Eg.

Photodegradation Kinetics of Rhodamin 6G

Photostability of Rhodamin 6G

To evaluate the photostability of Rh6G in the absence of catalyst, from a 1.15 mM stock solution of Rh6G, 5 uM Rh6G solutions were freshly prepared and irradiated for 90 min in a Solsim-Luzchem photoreactor using either UV lamps (8 Hitachi FL8BL-B lamps, 365 nm, 8W rated power consumption) or white light lamps (8 Westinghouse 4000K white light T5BF-840 lamps, 8W rated power consumption). Aliquots of the samples were taken every 10 min and their absorbance was measured at 526 nm in an Agilent 8453 UV-Vis spectrophotometer. The same procedure was performed incorporating additives (H_2O_2, NaCl, Na_2SO_4) to the Rh6G solutions. All the solutions were prepared using ultrapure water and the determinations were performed by triplicate unless otherwise indicated.

For the Raschig rings-supported TiO_2 catalysts, the photodegradation procedure involve the addition of 10 catalyst-coated Raschig rings to the Rh6G solutions, and keeping the same irradiation protocol previously described for the samples in homogenenous media.

Degradation of Rh6G in aqueous suspensions of TiO_2 took place under constant irradiation for 30 min. For comparison sake, the amount of TiO_2 used in the studied suspensions was determined by comparison with the mass of supported catalysts in the experiments involving the Raschig rings.

All the degradation kinetic data was adjusted to a pseudo-first order kinetic model, according to the Langmuir-Hinshelwood kinetic model for reactions taking place in heterogeneous media (Loghambal et al., 2018). All of the kinetics were performed under constant air bubbling. The reported data correspond to the average of at least three independent determinations, unless otherwise stated.

Evaluation of the chemical oxygen demand for the photodegradation of Rhodamin 6G.

The determination of the chemical oxygen demand was performed over the remainder organic matter left after a short photocatalytic degradation course (ca. 10 min). To a tube containing $K_2Cr_2O_7$, sulfuric acid and silver as a catalyst, 1 mL of a centrifuged solution of Rh6G previously subjected to photodegradation were added. The sample tubes were subjected to digestion at 150°C for 2 hrs. Once the samples are cooled, the concentration of Cr^{+3} was determined by spectrophotometric analysis, measuring the absorbance of the samples at 620 nm (Lenore et al., 2009). Reported results correspond to samples ($n = 3$) measured by triplicate, where the results were deemed suitable when their standard error were under 10% of the average value determined.

RESULTS AND DISCUSSION

TiO_2 Catalysts Characterization

TiO_2 catalysts were synthesized by a Sol-Gel method, starting by the hydrolysis of the metallic alcoxide, followed by calcination of the resulting gel (**Scheme 1**). The hydrolytic step was performed in acid media, resulting in 90% yield for the reaction.

$$Ti(i-oPr)_4 + H_2O \dot{\rightarrow} Ti(OH)_4 + 4HO - Pr$$

$$Ti(OH)_4 \overset{\Delta}{\rightarrow} TiO_{2(prep)} + 2H_2O$$

SCHEME 1 | Chemical reactions involved in the synthesis of the studied TiO_2 catalysts.

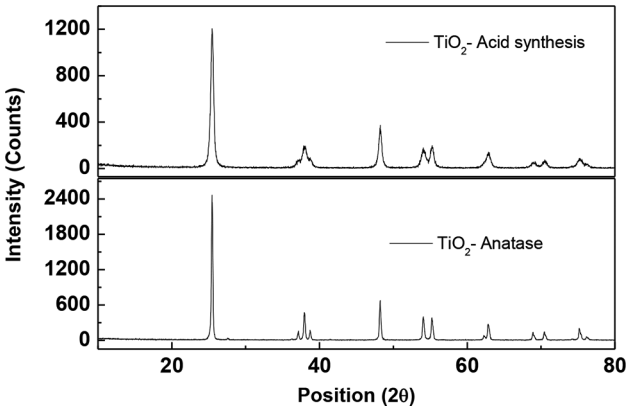

FIGURE 1 | X-ray powder diffraction pattern for the studied TiO_2 catalysts.

$$Ti(i-oPr)_4 + H_2OTi(OH)_4 + 4HO - Pr$$
$$Ti(OH)_4TiO_{2(prep)} + 2H_2O$$

X-ray diffraction analysis (**Figure 1**) of the synthesized TiO_2 catalysts herein named as acid synthesis TiO_2 (AS-TiO_2), show identical spatial features for the crystal structures of AS-TiO_2 and Anatase, with signals for AS-TiO_2 at 2θ values equals to: 25.4; 37.2; 37.9; 38.7; 48.2; 54.2; 55.3; 62.9; 69.0; 70.5; 74.1; 75.2, and 76.2. For Anatase is also observed the presence of minor signals (at values of 2θ equal to 27.6; 36.2 and 41.4), attributed to the presence of traces of the Rutil crystalline form of TiO_2, which are not observed in the XRD pattern of AS-TiO_2. The Rutil content in the commercial sample of Anatase is estimated as lower than 2%, according to calculations performed by using the relationship between the respective TiO_2 phase and the strongest reflection associated to each phase under consideration, according to: $phase\ \% = 100/(1+1.265I_R/I_A)$ (Spurr and Myers, 1957), where I_R and I_A are the respective intensities of the Anatase and Rutil signals at 2θ values of 25.1 and 27.6, respectively. For the Degussa P25 (DP25) samples, more intense signals at 2θ positions equivalent to those of Rutil are observed, associated with increased content of the Rutil crystalline phase in DP25, material comprised by the Anatase and Rutil phases of TiO_2 in an 85:15 ratio (See **Supplementary Figure 1** in the electronic supplementary information of this work, for the DP25 XRD pattern).

In order to establish further observations regarding the photocatalytic performance of the synthesized catalysts, their bandgap energy (Eg) was determined through diffuse refractance

measurements. **Figure 2** show diffuse refractance data plotted against the energy of the incident light, according to the Tauc modified Kubelka-Munk model (see methods for details). The values of Eg obtained for the synthesized catalyst (2.97 eV) are marginally lower than those determined for their commercial counterparts, with 3.03 eV and 3.17 eV for Degussa P25 and Anatase, respectively. The Eg results are in good agreement with the XRD data, particularly for the correspondence between AS-TiO_2 and Anatase structures. Considering that the energy of the bandgap for AS-TiO_2 is the lowest for the set of catalysts studied, and that the spectral response in the 250–400 nm range (**Figure 2**), between these catalysts is quite similar, it might be valid to expect for AS-TiO_2 to be particularly efficient when using white light in the photocatalytic process, by requiring

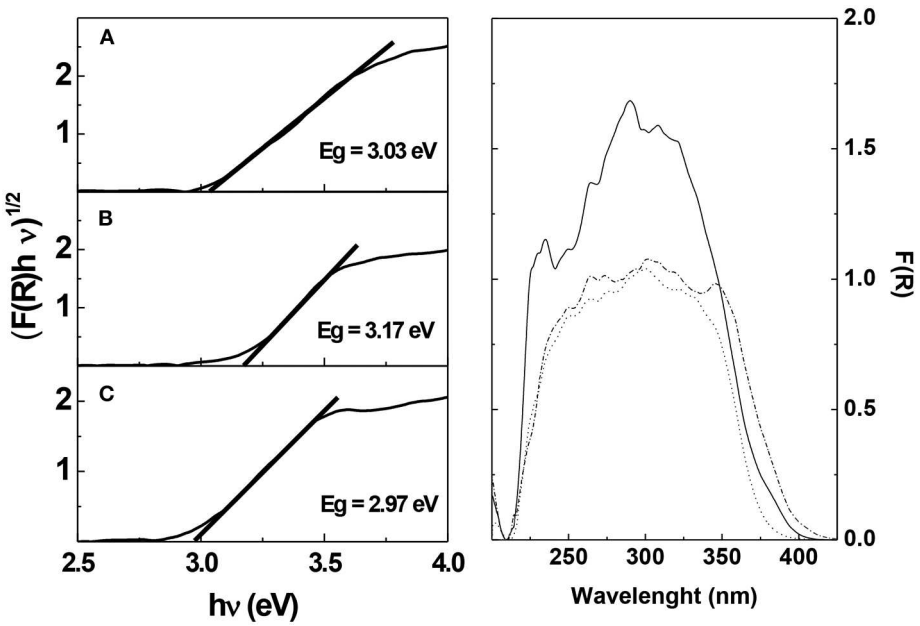

FIGURE 2 | (**Left**) Product between the diffuse refractance and the energy of the incident light represented against the energy of the incident light, according to the Tauc-modified Kubelka-Munk model. Linear regression for the determination of the bandgap energy is shown. Materials: (a) Degussa P25; (b) Anatase; (c) Acid synthesis TiO_2. (**Right**) Diffuse refractance spectra for the studied TiO_2 catalysts. (▬) Degussa P25; (●●●) Anatase; (-•-•-) Acid synthesis TiO_2.

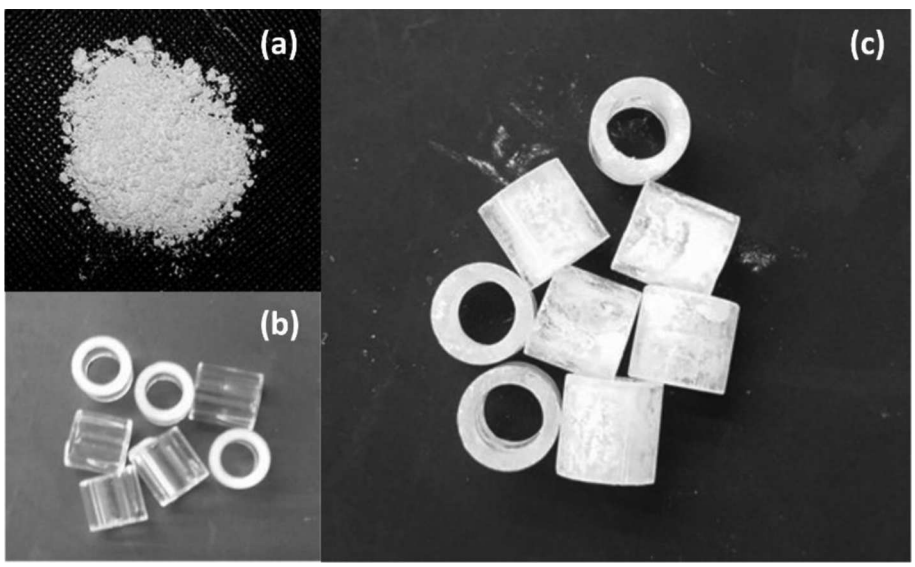

FIGURE 3 | (a) Synthesized TiO_2 catalyst. **(b)** Raschig rings without treatment. **(c)** Treated Raschig rings displaying supported TiO_2 catalyst.

less energy for the valency band electrons to transition to the conduction band of the catalyst (UV/Vis spectra of RH6G as well as UV and White light radiant emission spectra are available in **Supplementary Figure 2**).

The synthesized TiO_2 catalysts (**Figure 3a**), as well as commercial TiO_2 samples (Degussa P25 and Anatase), all of them in the form a finely divided powder, were supported on Raschig rings (RR), made up of borosilicate glass (**Figure 3b**) of 5.0 mm of height, with 4.0 and 5.0 mm of internal and external diameter, respectively. The supporting procedure was based the solvent evaporation of a TiO_2 suspension containing PEGMA-treated raschig rings, leading to the formation of an stable homogeneous layer of TiO_2 on both the external and internal surfaces of the rings, as shown in **Figure 3c**.

The TiO_2 support took place with varied efficiencies (**Table 1**). An important difference is observed on the support efficiency (SE) between AS-TiO_2 (8% SE) and the commercial TiO_2 samples. Degussa P-25 with a 20% SE and Anatase displaying the highest SE (26%). The observed differences in SE reported point toward raschig rings TiO_2-loading variations based on granularity differences of the supported material, where the packing of the commercial TiO_2 samples differs to that synthesized material, leading to the formation of layer(s) of different density between the samples studied.

In order to further support the claims regarding the differences in SE between the different TiO_2 samples, physcochemical characterization of the materials were performed. SEM images reveal relevant differences between the considered TiO_2 photocatalysts. AS-TiO_2 samples (**Figure 4A**) display defined crystalline microparticulated aggregates formed by nanometric clusters which are identifiable at larger magnifications (>30 k X; See **Supplementary Figure 3**). On the contrary both Anatase (**Figure 4B**) and Degussa P25 (**Figure 4C**) present a more disperse configuration, without the evidence of important cluster formation or identifiable discrete crystalline formations of micrometric dimensions. From N_2 adsorption/desorption isotherms evaluated under the BET model considerations, data shows (**Table 2**) that both AS-TiO_2 and Anatase share a similar adsorption performance with similar specific adsorption area, in the range from 60 to 65 m^2 per gram of adsorbent, whereas Degussa P25 shows a lower specific area, below 50 m^2 per gram of adsorbent. Regarding the porosity of the systems, AS-TiO_2 average pore size locates the material closer to the micro-mesoporous regime. Anatase on the other hand, operates on the mesoporous range, with an average pore size that is twice as large as that of AS-TiO_2 and nearly half of the average pore size determined for Degussa P25 (nearly 40 nm) indicating that the porosity regime of the latter leans toward the mesoporous/macroporous range.

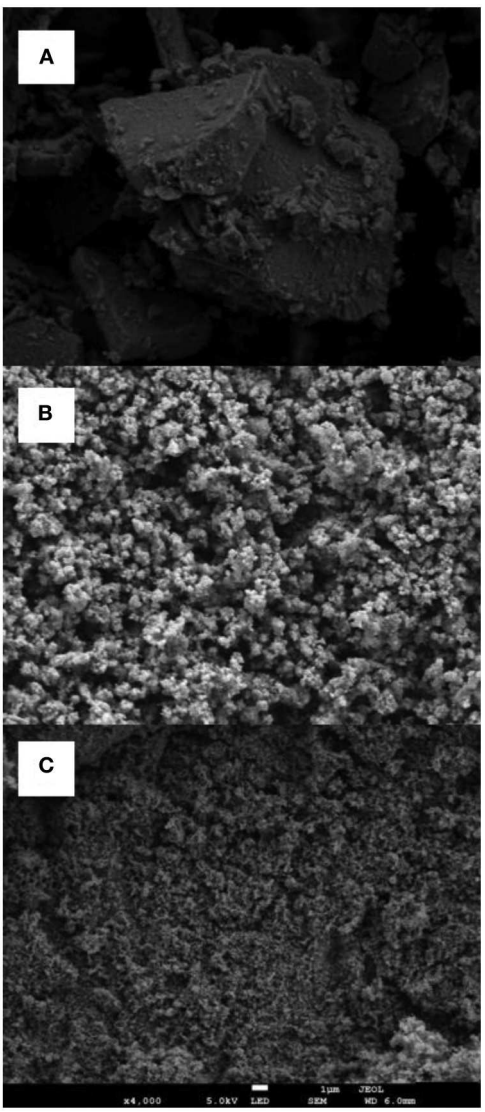

FIGURE 4 | Scanning electron microscopy characterization of the studied TiO_2 photocatalysts: **(A)** Acid synthesis TiO_2; **(B)** Anatase; **(C)** Degussa. Magnification: 4000X, Beam energy: 5,0 kV.

TABLE 1 | Support efficiency data for the thermal deposition of TiO_2 catalysts on borosilicate Raschig rings (Refer to methods section for further details).

TiO_2 catalyst	Support efficiency (%)
Degussa P25	20.1
Anatase	26.1
TiO_2 (acid synthesis)	8.3

TABLE 2 | Specific surface area (S_{BET}) of the studied TiO_2 photocatalysts, according to the Brunnauer, Emmet and Teller mode.

Sample	S_{BET} (m^2/g)	Pore diameter (nm)
AS-TiO_2	60.5	7.1
Anatase	65.9	18.9
Degussa P25	49.0	43.4

Textural identity is expressed as average pore diameter of the samples.

TABLE 3 | Kinetic data for the photodegradation of Rh6G in homogeneous media and in the presence of supported TiO_2 catalysts.

Light source/catalyst[a]	k_{obs} (min^{-1})	Degradation percentage
UV (365 nm)	$1.7\times10^{-2} \pm 2.9 \times 10^{-3}$	21.9 ± 3.2
UV (365 nm)/Degussa P25	$2.1 \times 10^{-2} \pm 6.7 \times 10^{-3}$	57.3 ± 6.8
UV (365 nm)/Anatase	$2.2 \times 10^{-2} \pm 1.4 \times 10^{-2}$	75.1 ± 3.0
UV (365 nm)/TiO_2 acid synthesis	$2.5 \times 10^{-2} \pm 9.0 \times 10^{-3}$	77.5 ± 7.8
White light	$2.0 \times 10^{-2} \pm 5.6 \times 10^{-3}$	22.9 ± 4.3
White light/Degussa P25	$4.0 \times 10^{-2} \pm 7.8 \times 10^{-3}$	27.1 ± 4.7
White light/Anatase	$2.6 \times 10^{-2} \pm 3.1 \times 10^{-3}$	36.8 ± 5.2
White light/TiO_2 acid synthesis	$3.1 \times 10^{-2} \pm 4.5 \times 10^{-3}$	66.8 ± 11.9

[a] *Experiments performed using 10 TiO_2-loaded Raschig rings.*

Photodegradation of Rhodamin 6G by Raschig Rings-Supported TiO_2

The photostability of Rh6G was studied in homogenous media by irradiating aqueous solutions of Rh6G using different light sources. The experimental configuration for the irradiation of the aqueous solutions of Rh6G, in the absence and the presence of supported catalysts, comprises a vertically-oriented sealed borosilicate glass tube located in a photoreactor with a series of lamps (UV or white light) lined up equally at each side of the tube (see **Supplementary Figure 4**), in order to achieve a total homogenous irradiation of the samples. Rh6G degradation kinetic data and degradation efficiency are shown in **Table 3**. The decrease of Rh6G concentration vs. time data behaved in accord to the pseudo-first order treatment (monoexponential decay), according to the Langmuir-Hinshelwood model for kinetics in solid-liquid interfaces and the kinetic profiles are shown in **Supplementary Figure 5** of this work.

When UV light (365 nm) is used to irradiate a solution of Rh6G a degradation percentage of 22% is determined, efficiency that is further increased in the presence of supported TiO_2 catalysts, with a near three-fold increase for Degussa P25 and a four-fold increase for Anatase and AS-TiO_2 with Rh6G degradation efficiencies above 70%. Similarly, the degradation rate is improved in the presence of the supported catalysts, with AS-TiO_2 displaying the highest degradation rate.

The degradation efficiency of Rh6G in solutions irradiated with white light (23%) is quite similar to that observed with UV light irradiated samples (22%). For the supported catalysts, particularly for Degussa P25 and Anatase, the degradation efficiency observed is lower (compared to UV light) when white light is used to irradiate the samples, with no significative differences between the degradation of Rh6G in homogeneous media compared to heterogeneous media using Degussa P25 as catalyst. Similarly, only a moderate enhancement of the degradation efficiency is observed when Anatase is used. Interestingly, the performance of the AS-TiO_2 supported catalyst is particularly good when irradiated with white light, inducing a three-fold increase on the degradation efficiency of Rh6G, increase that is only marginally lower than that observed with UV light.

Regarding the degradation rates observed for the white light irradiated samples, the analysis is not as straightforward as for UV light, with all of the catalysts moderately increasing the rate over the value observed in homogeneous media, with Degussa P25 doubling the degradation rate, followed by AS-TiO_2, and Anatase having almost no difference with the rate determined in homogenous media. In homogeneous media, namely in the absence of TiO_2, Rh6G absorbs light, undergoing a transition to its triplet state, in which this state Rh6G can release the energy and return to its ground state, get decomposed by photolysis or it can react with O_2 and generate singlet oxygen ($^1O_2$), which then can react with Rh6G leading to the formation of oxidation products. In the presence of the catalysts, the process becomes more complex, with the dye-mediated sensitization process and the intrinsic ability of TiO_2 working in tandem to generate ROS, which then readily contributes toward the degradation of Rh6G, further potentiating the photocatalytic process. From this, some observations can be made from the data in **Table 2**:

a) In the absence of TiO_2, degradation rates are similar irrespective of the light source used, indicating that the decomposition of Rh6G observed takes place by photolysis of the dye rather than ROS-induced oxidation.
b) When UV light is used the degradation of the dye takes place mainly by ROS generated due to the intrinsic photocatalytic activity of TiO_2 and by that induced by photosensitization, in all the TiO_2 variants studied.
c) The synthesized TiO_2 catalytic performance is slightly superior to its commercial counterpart (Anatase) when UV light is used, but greatly improves when visible light is used, this is due mainly by the decrease on the Eg of the synthesized catalyst (compared to Anatase), reduced photolysis of the dye, as well the enhancement of the photosensitization process.

In a comparison between the performance of the supported TiO_2 catalysts, and an equivalent mass of TiO_2 catalyst in suspension, it is revealed that an important fraction of the photodegradation efficiency is preserved in the supported material, going from ∼80 to 90% of photodegradation for all the TiO_2 suspensions (**Table 4**) to a 77% (UV light) and 66% (white light) as maximum values of photodegradation (**Table 3**) achieved by the supported materials (AS-TiO_2 and Anatase). The main cause of the observed differences might be associated to a loss of effective area of the supported TiO_2 catalysts due to adsorption on the rings surface vs. the total surface availability of the suspended particles of TiO_2. The percentage of retained photocatalytic activity in the supported TiO_2 catalyst is particularly good, particularly when taking into account the large surface area of TiO_2 catalysts lost upon support on the raschig rings, fact that is especially evident for the AS-TiO_2, material which displays the lower support efficiency and morphologically differs the most from the others TiO_2 variants (Anatase and Degusa P25), as presented in **Figure 4**.

In order to delve further in to the photocatalytic processes of the systems studied, the chemical oxygen demand (COD) for the photocatalyzed decomposition Rh6G was evaluated. The determination of the COD of the photocatalytic process can provide useful information in these type of complex oxidative

TABLE 4 | Kinetic data for the photodegradation of Rh6G on TiO_2 catalysts aqueous suspensions irradiated with UV light.

Catalyst[a]	k_{obs} (min^{-1})	Degradation percentage
Degussa P25	6.5×10^{-2}	80
Anatase	3.6×10^{-1}	89
TiO_2 acid synthesis	1.0×10^{-1}	91

[a] *Mass of suspended catalyst is determined as the equivalent mass of supported TiO_2 on 10 raschig rings.*

TABLE 5 | Chemical oxygen demand (COD) data for the photocatalytic degradation of Rhodamin 6G in the presence of supported TiO_2 catalysts irradiated with UV light.

Catalyst	COD (mg/L)	Degradation (%)
Degussa P25	20	25
Anatase	21	33
TiO_2 acid synthesis	21	33

TABLE 6 | Influence of additives on the kinetic data (21 °C) for the photodegradation of Rhodamin 6G in the presence of TiO_2 (acid synthesis) supported on Raschig rings.

Additive	k_{obs} (min^{-1})	Degradation percentage
UV light (365 nm)		
H_2O_2 (5 μM)	$1.9 \times 10^{-2} \pm 3.0 \times 10^{-3}$	60.1 ± 1.3
NaCl (5 μM)	$1.9 \times 10^{-2} \pm 4.0 \times 10^{-3}$	72.0 ± 2.6
Na_2SO_4 (5 μM)	$1.0 \times 10^{-2} \pm 1.9 \times 10^{-3}$	61.4 ± 8.8
NaCl (5 μM)/H_2O_2 (5 μM)	$2.5 \times 10^{-2} \pm 3.5 \times 10^{-3}$	63.3 ± 1.9
Na_2SO_4 (5 μM)/H_2O_2 (5 μM)	$2.4 \times 10^{-2} \pm 1.0 \times 10^{-3}$	68.6 ± 1.6
White light		
H_2O_2 (5 μM)	$1.7 \times 10^{-2} \pm 4.0 \times 10^{-3}$	51.6 ± 0.3
NaCl (5 μM)	$2.7 \times 10^{-2} \pm 4.2 \times 10^{-3}$	64.3 ± 6.9
Na_2SO_4 (5 μM)	$2.9 \times 10^{-2} \pm 4.0 \times 10^{-3}$	61.8 ± 5.6
NaCl (5 μM)/H_2O_2 (5 μM)	$1.8 \times 10^{-2} \pm 8.0 \times 10^{-3}$	55.4 ± 6.1
Na_2SO_4 (5 μM)/H_2O_2 (5 μM)	$2.5 \times 10^{-2} \pm 8.1 \times 10^{-3}$	59.3 ± 10.7

systems where parallel and sequential reactions might take place, systems in which common first order kinetics or initial rate kinetic methods might be somewhat limited to describe the overall process, particularly when spectrophotometric methods are used and the oxidative bleaching of the target molecule may not fully correspond with the whole oxidative pathway of said molecule (Mills et al., 2012). Similarly, COD has been successfully used in comparative studies involving semiconductor photocatalysts (El-Mekkawi et al., 2016). Data in **Table 5** shows COD values and Rh6D photodegradation percentages for the studied photocatalysts. The minor differences observed in the degradation percentages determined by COD in all of the supported TiO_2 variants, indicate that, besides the different complex photophysical processes taking place in various degrees, potentially involving different oxidation intermediaries, the endproducts of the considered photocatalytic systems appears to be similar.

Influence of Additives on the TiO_2-Catalyzed Photodegradation of Rhodamin 6G

The presence of additives and the study of their influence on the photocatalytic process is a matter of utmost importance, especially when considering the prospect of technological applications of the supported TiO_2 catalyst on waste water treatment, were salinity and the presence of oxidant agents may affect the performance of the catalysts. With this purpose, the addition of NaCl, Na_2SO_4, and H_2O_2 to the Rh6G solutions was considered, and their influence on the AS-TiO_2 photocatalytic activity was assessed (kinetic profiles in **Supplementary Figures 6, 7**). Data on **Table 6** shows that for H_2O_2 there is a decrease in the photodegradation efficiency (60%) compared to that in the absence of the additive (77%; **Table 3**) when UV light is used. Similarly, an almost equivalent decrease is observed when white light is used, with a 52 vs. 67% (**Table 3**) with and without H_2O_2 respectively. On the other hand, for NaCl, and for both of the light sources studied, a negligible decrease of the photodegradation efficiency is observed, with a 72% degradation with UV light and a 62 % for white light. As observed with NaCl, the addition of Na_2SO_4 induces no significative variation into the photodegradation efficiency observed with white light, contrary to a larger decrease when UV light is used, with a 62 and a 61% photodegradation with white light and UV light, respectively.

The kinetic data for the addition of H_2O_2 show a decrease on the rate constant (2.5×10^{-2} min^{-1} without H_2O_2; **Table 3**) for both light sources, whereas for SO_4^{-2} and Cl^- sodium salts there is no change in the rate constants when white light is used, but decreases when the samples are irradiated with UV light, with the largest decrease being observed for SO_4^{-2} (1.0×10^{-2} min^{-1}; **Table 6**).

Overall, the data presented regarding the influence of the SO_4^{-2}, Cl^- and hydrogen peroxide, shows a good tolerance of the photocatalytic system to these additives. The explanation for the observed influence of the anions in the system can be complex, for example both anions can interact with the vacant holes of the generated in the valence band, inhibiting the recombination of the hole/electron pair on the photocatalysts surface as well as to react with H_2O, generating hydroxyl radicals, leading to further degradation of Rh6G, however it has been also reported that these ions can also display an inhibitory behavior (Yan et al., 2012), by scavenging hydroxyl radicals generated on the surface of the catalyst, as well as by competing with Rh6G for the adsorption sites available, which seem to be the most likely explanation on the behavior of the data presented for the photodegradation of Rh6G in the studied system.

For the case of hydrogen peroxide, at nanomolar concentrations (Sahel et al., 2016; Kang et al., 2017), it can act as a scavenger of electrons from the conduction band of TiO_2, which promotes charge separation and the formation of hydroxyl radicals, which may lead to an enhanced degradation

of Rh6G. However, a decrease of photodegradation efficiency is observed in our system, indicating that at the considered H_2O_2 concentrations, electron and/or hydroxyl radical scavenging properties of hydrogen peroxide might be of relevance.

When equimolar ratios of H_2O_2 and salt are used, interesting results are observed. First, when UV light is used, the rate for the mixture $NaCl/H_2O_2$ is equal to that observed without additives, and higher than the values determined for the systems containing NaCl and H_2O_2 separately. On the contrary, for the samples irradiated with white light, the mixture shows a rate constant equal to that of the system containing only hydrogen peroxide, lower than the one determined in the absence of additives. The behavior observed for the samples containing the mixture Na_2SO_4/H_2O_2 is quite similar, for UV light, the rate of the photocatalytic process taking place in the presence of both SO_4^{-2} and H_2O_2 is higher than that of the additives separately, and equal to that observed in the absence of additives, the same being true for white light, but the rate of the mixture is now equal to that observed when Na_2SO_4 is the only additive present in the photocatalytic system.

CONCLUSIONS

Raschig rings-supported TiO_2 catalysts display a good photocatalytic performance when compared to equivalent amounts of TiO_2 in aqueous suspension, even though a large surface area of TiO_2 material is lost upon support. The comparative study between suspension vs. supported TiO_2 catalysts reveals that optimization of the available area in the raschig rings is imperative in order to improve the catalyzed photodegradation of Rh6G. This is particularly evident by taking into account that the characteristics (XRD, RD, Eg) and observed photodegradative performance of the synthesized catalysts are in good agreement with the commercial TiO_2 samples, and that the Rh6G photodegradation differences observed with the light sources considered are minimal in the presence of TiO_2 catalysts.

The presence of additives induce changes in the kinetics and efficiency of the TiO_2-catalyzed photodegradation of Rh6G, particularly when white light is used in the process, pointing toward a complex phenomenon, however the stability of the supported photocatalytic systems is acceptable in the presence of the studied additives. In line with this, the magnitude of the chemical oxygen demand, indicates that besides the different complex photophysical processes taking place, the intermediate products of the considered photocatalytic systems appears to be similar.

DATA AVAILABILITY STATEMENT

The raw data supporting the conclusions of this article will be made available by the authors, without undue reservation, to any qualified researcher.

AUTHOR CONTRIBUTIONS

EP designed the experiments, analyzed the results, and wrote and revised the manuscript. CC analyzed the results and wrote and revised the manuscript. FH and GA performed experimental activities. GC participated in the data analysis and discussions. All authors have approved the final revised manuscript.

FUNDING

This work was supported by DICYT-USACH 02184PL and Red CYTED318RT0551 grants.

ACKNOWLEDGMENTS

Universidad de Santiago de Chile, DICYT 02184PL, Vicerrectoria de investigación, desarrollo e innovación. Red CYTED318RT0551, University of Santiago of Chile. Thanks to the PAI: FQM 175 group directed by Dr. Julian Morales from the Department of Inorganic Chemistry and Chemical Engineering, School of Sciences, Campus Rabanales, University of Cordoba, Span.

SUPPLEMENTARY MATERIAL

The Supplementary Material for this article can be found online at: https://www.frontiersin.org/articles/10.3389/fchem.2020.00365/full#supplementary-material

REFERENCES

Ahmed, S., Rasul, M. G., Brownb, R., and Hashib, M. A. (2011). Influence of parameters on the heterogeneous photocatalytic degradation of pesticides and phenolic contaminants in wastewater: a short review. *J. Environ. Manage.* 92, 311–330. doi: 10.1016/j.jenvman.2010.08.028

Ajmal, A., Majeed, I., Malik, R. N., Idriss, H., and Nadeem, M. A. (2014). Principles and mechanisms of photocatalytic dye degradation on TiO_2 based photocatalysts: a comparative overview. *RSC Adv.* 4:37003. doi: 10.1039/C4RA06658H

Alahiane, S., Qourzal, S., El Ouardi, M., Abaamrane, A., and Assabbane, A. (2014). Factors influencing the photocatalytic degradation of reactive yellow 145 by TiO_2-coated non-woven fibers. *Am. J. Anal. Chem.* 5, 445–454. doi: 10.4236/ajac.2014.58053

Ali, S., Li, Z., Chen, S., Zada, A., Khan, I., Khan, I., et al. (2019). Synthesis of activated carbon-supported TiO_2-based nano-photocatalysts with well recycling for efficiently degrading high-concentration pollutants. *Catal. Today* 351. 557–564. doi: 10.1016/j.cattod.2019.03.044

Amenn, S., Akhtar, M. S., Seo, H-K., and Shin, H-S. (2013). Mineralization of rhodamine 6G dye over roseflower-like ZnO nanomaterials. *Mater. Lett.* 113, 20–24. doi: 10.1016/j.matlet.2013.09.004

Ansón-Casaos, A., Tacchini, I., Unzue, A., and Martínez, M. T. (2013). Combined modification of a TiO_2 photocatalyst with two different carbon forms. *Appl. Surf. Sci.* 270, 675–684. doi: 10.1016/j.apsusc.2013.01.120

Barranco, A., and Groening, P. (2006). Fluorescent plasma nanocomposite thin films containing nonaggregated rhodamine 6G laser dye molecules. *ACS J. Langumir Surf. Colloids* 22, 6719–6722. doi: 10.1021/la053304d

Bokhale, N. B., Bomble,S., Dalbhanjan, R. R., Mahale, D. D., Hinge,S. P., Banerjee,B. S., et al. (2014). Sonocatalytic and sonophotocatalytic degradation

of rhodamine 6G containing wastewaters. *Ultrason. Sonochem.* 21, 1797–1804. doi: 10.1016/j.ultsonch.2014.03.022

Bujdak, J., and Iyi, N. (2012). Highly fluorescent colloids based on rhodamine 6G, modified layered silicate and organic solvent. *J. Colloid Interf. Sci.* 388, 15–20. doi: 10.1016/j.jcis.2012.08.020

Carreon, M. L., Carreonet, H. G., Espino-Valencia, J., and Carreon, M. A. (2011). Photocatalytic degradation of organic dyes by mesoporous nanocrystalline anatase. *Mater. Chem. Phys.* 125, 474–478. doi: 10.1016/j.matchemphys.2010.10.030

Chong, M., Jin, B., Chow, W., and Saint,. C. (2010). Recent developments in photocatalytic water treatment technology a review. *Water Res.* 44, 2997–3027. doi: 10.1016/j.watres.2010.02.039

Daghrir, R., Droguie, P., Ka, I., El Khakanib, M. A. (2012). Photoelectrocatalytic degradation of chlortetracycline using Ti/TiO_2 nanostructured electrodes deposited by means of a pulsed laser deposition process. *J. Hazard. Mater.* 199-200, 15–24. doi: 10.1016/j.jhazmat.2011.10.022

Dyi-Hwa, T., Lain-Chuen, J., and Hsin-Hsu, H. (2012). Effect of oxygen and hydrogen peroxide on the photocatalytic degradation of monochlorobenzene in aqueous suspension. *Int. J. Photoenergy* 2012:328526. doi: 10.1155/2012/328526

El-Mekkawi, D. M., Galal, H. R., Abd EL Wahad, R. M., and Mohamed, W. A. A. (2016). Photocatalytic activity evaluation of TiO_2 nanoparticles based on COD analyses for water treatment applications: a standardization attempt. *Int. J. Environ. Sci. Technol.* 13, 1077–1088 doi: 10.1007/s13762-016-0944-0

Foo, K. Y., and Hameed, B. H. (2009). An overview of landfill leachate treatment via activated carbon adsorption process. *J. Hazard. Mater.* 171, 54–60. doi: 10.1016/j.jhazmat.2009.06.038

Fujishima, A., and Honda, K. (1972). Electrochemical photolysis of water at a semiconductor electrode. *Nature* 238, 37–38. doi: 10.1038/238037a0

Gaya, U. I. (2014). *Heterogeneous Photocatalysis Using Inorganic Semiconductor Solids*. Dordrecht: Springer. doi: 10.1007/978-94-007-7775-0

Giménez, J., Bayarri, B., González, O., Malato, S., Peral, J, and Esplugas, S. (2015). Advanced oxidation processes at laboratory scale: environmental and economic impacts. *ACS Sustain. Chem. Eng.* 3, 3188–3196. doi: 10.1021/acssuschemeng.5b00778

Guillard, C., Puzenat, E., Lachheb, H., Houas, A., and Herrmann, J. M. (2005). Why inorganic salts decrease the photocatalytic efficiency. *Int. J. Photoenergy* 7:641208. doi: 10.1155/S1110662X05000012

Hurum, D. C., Agrios, A. G., and Gray, K. A. (2003). Explaining the enhanced photocatalytic activity of degussa P25 mixed-phase TiO_2 using EPR. *J. Phys. Chem. B* 107, 4545–4549. doi: 10.1021/jp0273934

Kang, S., Zhang, L., Liu, C., Huang, L., Shi, H., and Cui, L. (2017). Hydrogen peroxide activated commercial P25 TiO_2 as efficient visible-light-driven photocatalyst on dye degradation. *Int. J. Electrochem. Sci.* 12, 5284–5293 doi: 10.20964/2017.06.54

Landmann, M., Rauls, E., and Schmidt, W. G. (2012). The electronic structure and optical response of rutile anatase and brookite TiO_2. *J. Phys.* 24, 195503–195508. doi: 10.1088/0953-8984/24/19/195503

Lasio, B., Malfatti, L., and Innocenzi, P. (2013). Photodegration of rhodamine 6G dimers in silica sol-gel films. *J. Photochem. Photobiol A Chem.* 271, 93–98. doi: 10.1016/j.jphotochem.2013.08.007

Lenore, S., Clescerl Arnold, E., and Greenberg Andrew, D., Eaton. (2009). *Standard Methods for Examination of Water & Wastewater, 20th Edn*. Washington, DC: American Public Health Association.

Li, X., Chen, C., and Zhao, J. (2001). Mechanism of photodecomposition of H_2O_2 on TiO_2 surfaces under visible light irradiation. *Langmuir* 17, 4118–4122. doi: 10.1021/la010035s

Liu, G., Wang, G., Hu, Z., Su, Y., and Li, Z. (2019). Ag_2O nanoparticles decorated TiO_2 nanofibers as a p-n heterojunction for enhanced photocatalytic decomposition of RhB under visible light irradiation. *Appl. Surf. Sci.* 465, 902–910. doi: 10.1016/j.apsusc.2018.09.216

Loghambal, S., Agvinos Catherine, A. J., and Velu Subash, S. (2018). Analysis of langmuir-hinshelwood kinetics model for photocatalytic degradation of aqueous direct blue 71 through analytical expression. *Int. J. Math. Appl.* 6, 903–913.

López, R., and Gómez, R. (2012). Band-gap energy estimation from diffuse reflectancemeasurements on sol–gel and commercial TiO_2: a comparative study. *J. Sol. Gel Sci. Technol.* 61, 1–7. doi: 10.1007/s10971-011-2582-9

Magde, D., Rojas, G. A., and Seybold, P. G. (1999). Solvent dependence of the fluorescence lifetimes of xanthene dyes. *Photochem. Photobiol.* 70, 737–744. doi: 10.1111/j.1751-1097.1999.tb08277.x

Mahshid, S., Askari, M., and Sasani Ghamsari, M. (2007). Synthesis of TiO_2 nanoparticles by hydrolysis and peptization of titanium isopropoxide solution. *J. Mater. Process. Technol.* 189, 296–300. doi: 10.1016/j.jmatprotec.2007.01.040

Malesic-Eleftheriadou, N., Evgenidou, E. N., Kyzas, G. Z., Bikiaris, D. N., and Lambropoulou, D. A. (2019). Removal of antibiotics in aqueous media by using new synthesized bio-based poly(ethyleneterephthalate)-TiO_2 photocatalysts. *Chemosphere* 234. 746–755. doi: 10.1016/j.chemosphere.2019.05.239

Mills, A., Hill, C., and Robertson, P. K. J. (2012). Overview of the current ISO tests for photocatalytic materials. *J. Photochem. Photobiol. A* 237, 7–23 doi: 10.1016/j.jphotochem.2012.02.024

Módenes, A. N., Espinoza-Quiñones, F. R., Manenti, D. R., Borba, F. H., Palácio, S. M., and Colombo, A. (2012). Performance evaluation of a photo-fenton process applied to pollutant removal from textile effluents in a batch system. *J. Environ. Manage.* 104, 1–8. doi: 10.1016/j.jenvman.2012.03.032

Ochoa, Y., Ortegón, Y., Vargas, M., and Rodríguez, J. (2009). Síntesis de TiO_2, fase anatasa, por el método Pechini. *Suplemento de la Revista Latinoamericana de Metalurgia y Materiales* 3, 931–937.

Raja, P., Bensimon, M., Kulik, A., Foschia, R., Laub, D., Albers, P., et al. (2005). Dynamics and characterization of an innovative raschig rings–TiO_2 composite photocatalyst. *J. Mol. Catal. A Chem.* 237, 215–223. doi: 10.1016/j.molcata.2005.04.060

Ranjith, R., Renganathan, V., Chen, S. M., Selvan, N. S., and Rajam, P. S. (2019). Green synthesis of reduced graphene oxide supported TiO_2/Co_3O_4 nanocomposite for photocatalytic degradation of methylene blue and crystal violet. *Ceram. Int.* 45, 12926–12933. doi: 10.1016/j.ceramint.2019.03.219

Rejek, M., and Grzechulska-Damszel, J. (2018). Degradation of sertraline in water by suspended and supported TiO_2. *Pol. J. Chem. Technol.* 20, 107–112. doi: 10.2478/pjct-2018-0030

Rizzo, L., Meric, S., Guida, M., Kassinos, D., and Belgiorno, V. (2009). Heterogenous photocatalytic degradation kinetics and detoxification of an urban wastewater treatment plant efluents contaminated with pharmaceuticals. *Water Res.* 43, 4070–4078. doi: 10.1016/j.watres.2009.06.046

Robinson, T., McMullan, G., Marchant, R., and Nigam, P. (2001). Remediation of dyes in textile effluent: a critical review on current treatment technologies with a proposed alternative. *Bioresour. Technol.* 77, 247–255. doi: 10.1016/S0960-8524(00)00080-8

Rodríguez, E. M., Rey, A., Mena, E., and Beltrán, F. J. (2019). Application of solar photocatalytic ozonation in water treatment using supported TiO_2. *Appl. Catal. B Environ.* 254, 237–245. doi: 10.1016/j.apcatb.2019.04.095

Sahel, K., Elsellami, L., Mirali, I., Dapozze, F., Bouhent, M., and Guillard, C. (2016). Hydrogen peroxide and photocatalysis. *Appl. Catal. B Environ.* 188, 106–112. doi: 10.1016/j.apcatb.2015.12.044

Smith, A. M., and Nie, S. (2009). Semiconductor nanocrystals: structure, properties, and band gap engineering. *Acc. Chem. Res.* 43, 190–200. doi: 10.1021/ar9001069

Song, H., Chen, C., Zhang, H., and Huang, J. (2016). Rapid decolorization of dyes in heterogeneous fenton-like oxidation catalyzed by Fe-incorporated Ti-HMS molecular sieve. *J. Environ. Chem. Eng.* 4, 460–467. doi: 10.1016/j.jece.2015.12.003

Spurr, R. A., and Myers, H. (1957). Quantitative analysis of anatase-rutile mixtures with an X-ray difractometer. *Anal. Chem.* 29, 760–762. doi: 10.1021/ac60125a006

Stracke, F., Heupel, M. A, and Thiel, E. (1999). Singlet molecular oxygen photosensitized by Rhodamine dyes: correlation with photophysical properties of the sensitizers. *J. Photochem. Photobiol. A Chem.* 126, 51–58. doi: 10.1016/S1010-6030(99)00123-9

Sun, S., Zhao, R., Xie, Y., and Liu, Y. (2019). Photocatalytic degradation of aflatoxin B_1 by activated carbon supported TiO_2 catalyst. *Food Control* 100, 183–188. doi: 10.1016/j.foodcont.2019.01.014

Tarud, F., Aybar, M., Pizarro, G., Cienfuegos, R., and Pastén, P. (2010). Integrating fluorescent dye flow-curve testing and acoustic doppler velocimetry profiling for *in situ* hydraulic evaluation and improvement of clarifier performance. *Water Environ. Res.* 82, 675–685. doi: 10.2175/106143009X425889

Teoh, W. Y., Scott, J. A., and Amal, R. (2012). Progress in heterogeneous photocatalysis: from classical radical chemistry to engineering nanomaterials and solar reactors. *J. Phys. Chem. Lett.* 3, 629–639. doi: 10.1021/jz3000646

Vanamudan, A., and Pamidimukkala, P. (2015). Chitosan, nanoclay and chitosan–nanoclay composite as adsorbents for rhodamine-6G and the resulting optical properties. *Int. J. Biol. Macromol.* 74, 127–135. doi: 10.1016/j.ijbiomac.2014.11.009

Wan, X., Ke, H., Yang, G., and Tang, J. (2018). Carboxyl-modified hierarchical wrinkled mesoporous silica supported TiO_2 nanocomposite particles with excellent photocatalytic performances. *Prog. Nat. Sci. Mater. Int.* 28, 683–688. doi: 10.1016/j.pnsc.2018.11.007

Wang, J., Wang, G., Wei, X., Liu, G., and Li, J. (2018). ZnO nanoparticles implanted in TiO_2 macrochannels as an effective direct Z-scheme heterojunction photocatalyst for degradation of RhB. *Appl. Surf. Sci.* 456, 666–675. doi: 10.1016/j.apsusc.2018.06.182

Wu, T., Liu, G., and Zhao, L. (1998). Photoassisted degradation of dye pollutants. V. self-photosensitized oxidative transformation of rhodamine B under visible light irradiation in aqueous TiO_2 dispersions. *J. Phys. Chem. B* 102, 5845–5851. doi: 10.1021/jp980922c

Yan, X., Bao, R., Yu, S., Li, Q., and Jin, Q. (2012). The roles of hydroxyl radicals, photo-generated holes and oxygen in the photocatalytic degradation of humic acid. *Russ. J. Phys. Chem.* 86, 1479–1485. doi: 10.1134/S0036024412070333

Yaseen, D. A., and Scholz, M. (2019). Textile dye wastewater characteristics and constituents of synthetic effluents: a critical review. *Int. J. Environ. Sci. Technol.* 16, 1193–1226. doi: 10.1007/s13762-018-2130-z

Zehentbauer, F. M., Moretto, C., Stephen, R., Thevar, T., Gilchrist, J. R., Pokrajac, D., et al. (2014). Fluorescence spectroscopy of rhodamine 6G: concentration and solvent effects. *Spectrochim. Acta A Mol. Biomol. Spectrosc.* 121, 147–151. doi: 10.1016/j.saa.2013.10.062

Conflict of Interest: The authors declare that the research was conducted in the absence of any commercial or financial relationships that could be construed as a potential conflict of interest.